JOURNAL OF THERMOPHYSICS AND HEAT TRANSFER
Vol. 37, No. 4, October–December 2023

Technical Notes

Recurrent Neural Network Flow Rate Modeling of Piezoelectric Injectors in Cooling Testbeds

Andrew G. Fordon,* Fernando Soria,† Yunjun Xu,‡ and Shawn A. Putnam§
University of Central Florida, Orlando, Florida 32826

https://doi.org/10.2514/1.T6833

I. Introduction

THE energy, transportation, and manufacturing sectors require advanced cooling methods to meet their challenging thermal management demands. Spray cooling is established as one of the most efficient methods of cooling heated surfaces due to its ability to remove high heat fluxes [1]. For example, spray cooling has contributed to a profound 30% size reduction between Apple's A10 and A11 chips [2]. Cooling with continuous water sprays can dissipate heat flux up to 1000 W/cm^2, whereas pulsing sprays result in an improved heat transfer due to an increase in film evaporation during periods of no spray [3]. Moreover, increasing the number of nozzles leads to a superior critical heat flux (CHF) for a given mass flow rate [4]. For instance, applying multinozzle spray cooling in nuclear reactor powerplants was shown to achieve a heat flux margin of 2.97 W/cm^2 [5]. A coordinated high-pressure multinozzle spray improves the cooling uniformity and avoids warping by making mechanical, thermal, and chemical properties more consistent over large surfaces [4].

To study the unknown heat transfer limits of multinozzle spray cooling, it is necessary to construct a testbed. To date, low-pressure spray cooling testbeds with one nozzle [3,6,7] have been built to explore surface impaction, film formation, nucleate boiling regimes, and CHF. Another example developed an experimental setup to study system-level impingement cooling with cryogens [8]. Conversely, common rails are extensively employed in diesel fuel injection systems to accumulate high-pressure fuel before injection, ensuring that each nozzle has the same pressure and an equal flow rate [9–11]. Therefore, by employing a common rail, a unform and high-pressure environment is created, enabling equal flow rates and droplet sizes to be maintained across all nozzles that are required by the multinozzle, pulsed spray cooling system. The diesel fuel direct injection testbeds presented in Refs. [12,13] used experimental results to investigate fault detection and output rotational speed, respectively. Furthermore, a mathematical model describing the relationships among the input and output variables is necessary when designing advanced controllers for such multinozzle spray testbeds.

Models of common-rail systems can be categorized as system level (meaning from a macroperspective) or component level (meaning from a subsystem perspective). Due to the complexity of the involved hydrodynamic and electromagnetic processes, piezoelectric-based common-rail systems are typically modeled using component-level approaches with varying fidelity levels. For example, the model in Ref. [9] describes correlations between piezoelectric characteristics and the injection flow rate, whereas the model in Ref. [10] uses continuity relations to estimate the fuel injection mass flow rate and needle lift. Both results are validated via the Bosch method [9,10], in which the injection flow rate is found by measuring the dynamic pressure of the fluid out of an injector nozzle. In the Bosch method, the injector is encapsulated in a fixture with a dynamic pressure transducer, which is then attached to a coil of tubing filled with fluid [9,10]. The injector flow rate can be realized by measuring the pressure increase inside the coil; however, this cannot be extended to a real cooling scenario where the injector cannot be encapsulated [9,10]. Furthermore, analytical piezoelectric injector models are unrealizable because of undisclosed manufacturing parameters. Other common-rail subsystem models have achieved promising forecasts of pressure fluctuation on a common rail controlled by the electric control unit [11,14]. In contrast, system-level models of a diesel engine approximated ignition, combustion, and emission parameters [15,16].

Common-rail-based systems can be modeled using either physical laws or data-driven approaches. Thus far, common-rail injection has been frequently modeled via physical laws [9–11]. However, many assumptions and approximations are involved in these models, with transient dynamics and practical hardware constraints generally omitted for simplicity. For example, the piezoelectric model in Ref. [10] contains numerous assumptions regarding temperature effects and needle actuation events. Contrarily, a data-driven model applied two-dimensional bilinear interpolation mapping to predict Nitrogen Oxide and diesel engine soot emissions that achieved excellent results when compared to experimental data [17].

Neural networks (NNs), as one branch of data-driven modeling methods, have gained prevalence with improved machine learning techniques and increased computational power. Specifically, neural network models of common-rail injection and spray cooling show promising representations of nonlinearities and transient effects over the aforementioned physical law-based models. For instance, a recurrent neural network (RNN) model was able to relate the duty cycles of neighboring injectors to preinjection common-rail pressure fluctuations [14]. Likewise, a model of continuous, multinozzle spray cooling in casting processes via a convolution recurrent neural network predicted temperature profiles on a cooling surface [18]. In Ref. [19], an artificial NN (ANN) was superior to computational fluid dynamics when modeling spray cooling parameters in three boiling regimes. Furthermore, data-driven NN models have a preferable ability to represent system-level processes rather than focusing on subsystem components. The testbed model presented in Ref. [20] had better resolution, as compared to the physical emissions models in Refs. [15,16], by employing two sequentially connected neural networks for predicting the relationship between common-rail injection parameters and emission indices. Similarly, Ref. [3] modeled a pulsed spray cooling testbed, with a constant nozzle pressure (2 bar), using a classification ANN to predict the heat flux from the surface temperature, duty cycle, and pulse width modulation (PWM) frequency. Lastly, a neural network modeled the temperature uniformity of a near-space-oriented spray cooling testbed [21], achieving a 7% maximum relative error.

In this study, an RNN is used to model the time-sequential relationship between the input (e.g., PWM signals and common-rail pressure)

Received 28 February 2023; revision received 2 May 2023; accepted for publication 2 June 2023; published online 5 July 2023.

*Graduate Research Assistant, Department of Mechanical and Aerospace Engineering; Afordon318@knights.ucf.edu.
†Graduate Research Assistant, Department of Mechanical and Aerospace Engineering; Fsoria0408@knights.ucf.edu.
‡Professor, Department of Mechanical and Aerospace Engineering; Yunjun.Xu@ucf.edu. Associate Fellow AIAA.
§Associate Professor, Department of Mechanical and Aerospace Engineering; Shawn.Putnam@ucf.edu.

and the output (e.g., injector volumetric flow rate) of an accumulator-common-rail-injection subsystem. This subsystem is part of a recently built multinozzle spray cooling testbed. This testbed consists of a high-pressure common rail with two piezoelectric injectors controlled by PWM signals, an accumulator, a water reservoir, and a heating assembly.

To the best knowledge of the authors, this is the first effort of modeling a piezoelectric injector in a common-rail-based multispray cooling testbed using an RNN. The advantages of the approach are summarized as follows.

1) The data-driven approach avoids approximations and assumptions required in physical law modeling approaches.

2) Practical challenges observed in the testbed, such as the head loss between the accumulator and the common rail, can be mitigated using the RNN modeling method.

3) An RNN model can recognize trends in sequential data and identify its temporal order [22].

4) Trends of the volumetric flow rate for the cooling process can be predicted in real time with an accurate RNN model, where the Bosch method [9,10] falls short.

5) The data-driven RNN model bypasses the analytical model's need for manufacturer data.

This Technical Note is organized as follows. Section II briefly discusses the testbed: particularly the accumulator-common-rail-injector subsystem. The parameter relationships and the RNN structure are discussed in Sec. III. Section IV shows the experiment settings along with the training, validation, and test results of the RNN model using experimental data. Finally, conclusions are given in Sec. V.

II. Experimental Testbed

Figure 1 shows a schematic and image of the multinozzle spray cooling testbed. The working fluid is distilled water at room temperature. The BMW® common rail is filled from a 2 gal reservoir at 300 psi through a low-pressure PM® 190 liter lifting pump and sifted by a 100 μm filter. Subsequently, a valve closes the system from the reservoir. The system is then pressurized by the 2.5 gal accumulator using a continuous supply of air acting on the bladder from the high-pressure 2.26 ft^3 air tank. Various pressure settings over the range of 900–2500 psi, controlled by a pressure regulator, are used to determine its effects on the system output (i.e., the injector volumetric flow rate). The National Instruments (NI) cRIO 9056 controller and NI 9751 driver module send PWM signals to two piezoelectric N54 injectors positioned along the common rail. The injectors are positioned horizontally, 3 in. perpendicular to the heating plate and 6 in. parallel to one another.

The pressure of the common rail is measured by an Ashcroft® G2 transducer with an accuracy of ±0.25%. Signal processing and data accumulation are performed by a USB-6361 data acquisition board (DAQ) via LabView. The PWM injector control signals are measured using high-voltage probes via a MD04104C mixed domain oscilloscope, whereas the injected mass is measured by a JF-series analytical balance digital scale.

III. Volumetric Flow Rate Modeling via RNN

An RNN is constructed to model the continuous input–output relationship of the exit volumetric flow rate for the testbed's accumulator-common-rail-injector subsystem. The PWM waveform along with the common-rail pressure forms the inputs of model, whereas the output is the injector exit volumetric flow rate. These parameters are time series in nature, taken at each time step $t \in [t_0, \ldots, t_N]$. For the training, validation, and testing, the PWM and p_{CR} are directly measured; whereas the volumetric flow rate is calculated using the common-rail pressure and digital scale data.

The volumetric flow rate cannot be directly measured with flow meters because of the minuscule amount of volume being expelled by the injector per injection event (i.e., mostly on the order of 10 μL for spray durations lasting between 1 and 5 ms). Other methods for calculating the flow rate (e.g., the Bernoulli relation of the Poiseuille's law [23]) do not apply when considering that the injector exit pressure is unmeasurable. An attempt to measure the driving pressure between the accumulator and the common rail was influenced by the head loss resulting from the difference in height and length between locations. Additionally, measuring the pressure difference across the common rail had issues due to pressure fluctuations from a combination of transducer noise and the ensuing water hammer of injection actuation. Furthermore, calculating the flow rate exiting the accumulator with the ideal gas law [24] could produce the average flow rate of the total system but not the real-time injector flow rate.

As expected by the Poiseuille's law [23], a linear relationship was observed between the common-rail pressure and the mass expelled by an injector during a single-pulse event using a JF-series analytical balance digital scale. Applying this linear relationship, the following equation is proposed to approximate the mass expelled for a single injection event as

$$m(t) = \left[m_{\text{inj}} p_{\text{CR}_{\text{Drop}}}(t) - m_{\text{inj}} p_{\max}\right] / p_{\text{range}} \tag{1}$$

where m_{inj} is the total expelled mass measured by the digital scale as a single event at the end of the impulse, and $p_{\text{CR}_{\text{Drop}}}(t) = p_{\max} - p_{\text{CR}}(t)$ is the common-rail pressure drop at time t from its beginning. Note that $p_{\text{range}} = p_{\min} - p_{\max}$, where $p_{\max}$ and $p_{\min}$ represent the common-rail pressure at the beginning and end of an injection event, respectively. The volumetric flow rate is then calculated by taking the time derivative of $m(t)$ and dividing by the density as $\dot{Q}_{\text{Inj}} = \dot{m}(t)/\rho$, in which ρ is the water density. The pressure and, therefore, the flow rate are identical across multiple nozzles due to the use of the common rail. Therefore,

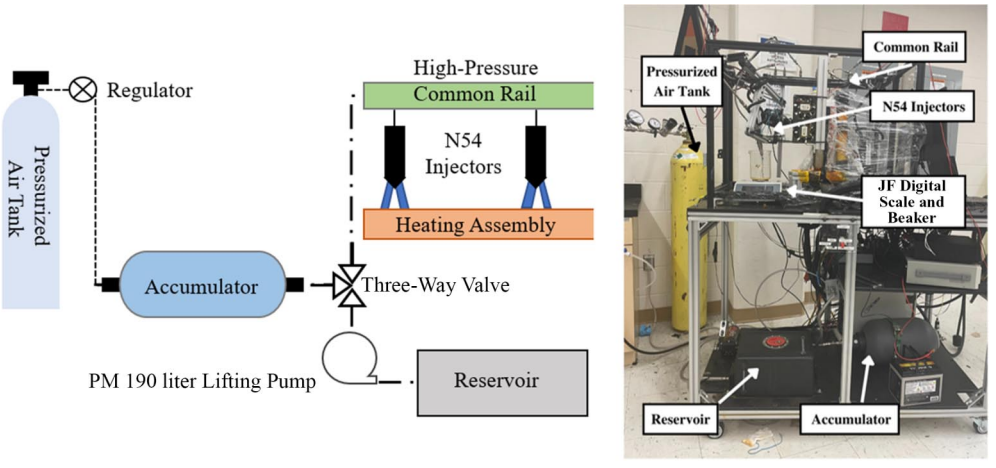

Fig. 1 Testbed schematic (Fig. 1a) and actual testbed (Fig. 1b). Flow of water is reservoir to accumulator to common rail to injector to hot surface. Flow of air is high-pressure air tank to regulator to accumulator.

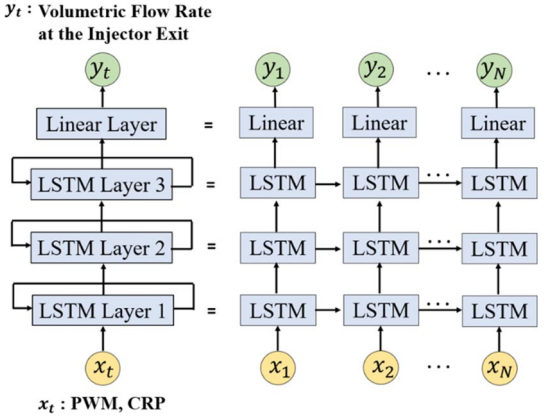

Fig. 2 RNN structure (customized based on Ref. [25]; CRP denotes common-rail pressure) unraveled through time: at each LSTM layer, information from both the current and previous time steps is used to make a prediction.

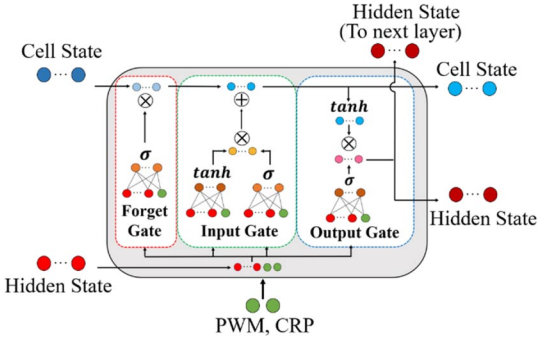

Fig. 3 LSTM structure (customized based on Ref. [25]): the current input of the PWM and CRP are concatenated with the encoded information from the previous time step, also known as the hidden state. Long-term information is encoded in the cell state, short-term information is encoded in the hidden state, and information deemed unimportant is forgotten.

the model describing the correlations between the PWM, the common-rail pressure, and the flow rate is independent of the number of nozzles.

The overall RNN structure is shown in Fig. 2 [25], where each time step has three long short-term memory (LSTM) [22] layers and one linear layer. The PWM signals and common-rail pressure at $t \in [t_0, \ldots, t_N]$ are the input to LSTM layer 1, and the outputs of the linear layer are the RNN's prediction of volumetric flow rate at the injector exit.

The LSTM cell, shown in Fig. 3 [25], helps mitigate the vanishing gradient issue and allows for enhanced capturing of long-term trends [22]. The values of the cell and hidden states are fed to the layer to predict the states of the next time step. The hidden state values also compose the LSTM layer's output and are passed as an input to the next LSTM layer. Finally, the hidden state output of the last LSTM layer will be the input to the linear layer.

The RNN is programmed using PyTorch® and runs on a laptop with an Intel Core i7 Processor and 15.8 GB of RAM. The network was trained via CUDA-GPU parallelization on a NVIDIA GeForce MX450 card.

IV. Experiment Setting, Results, and Discussion

A total of 85 experiments were conducted to study the relationship between the PWM signals, the common-rail pressure, and the volumetric flow rate. The PWM pulse width spanned between 1 and 5 ms, with increments of 1 ms. Similarly, the common-rail pressure ranged from 900 to 2500 psi, with increments of 100 psi. The PWM voltage was set to switch between 0 and 150 V during all cases; however, an error of ±5 V was measured. All experiments were performed at ambient room temperature and pressure.

The pressure and PWM measurements were taken at a sampling frequency of 2 kHz (a sampling period of 0.5 ms) and a time length of 12 ms, in which three trials of each experimental case were taken to increase validity. To reduce noise, a moving mean filter was applied to the raw pressure signal. The volumetric flow rate was then calculated for a total of 25 data points per experiment.

Among the 85 datasets, 75 were selected to form the training set that covered the range of experiment scenarios. The remaining 10 datasets formed the validation set (five datasets) and test set (five datasets). Although both the validation and test sets were not trained on, the validation set was used during the tuning process. The network was trained based on a given combination of the network size, loss function, and optimizer; it then made predictions on the validation set. These parameters were then updated based on the network's ability to recognize the trends, in addition to both the training and validation loss values. Once the network performed well on the validation set and a final tuned model was reached, predictions on the test set were made to offer an unbiased metric of performance.

Two solvers in PyTorch were tried, with the limited-memory Broyden–Fletcher–Goldfarb–Shanno [26] solver was shown to be superior to the Adam optimizer [26]. Similarly, the Huber loss [22] function demonstrated a preferable ability to model the impulsive data trends as compared to the mean squared error and the log loss functions, due to the fact that it is an adjustable squared loss and is less sensitive to outliers [22]. The layer sizes of 25, 50, 100, 250, 500, 550, 600, 650, 700, and 1000 were tried, in conjunction with fluctuating the number of layers between one, two, three, and four. Among these combinations, the best network configuration was three layers with sizes of 650, 25, and 25, respectively.

The training converged to a loss value of 2.059×10^{-3} after 60 training iterations (i.e., epochs). The five validation datasets and five test datasets converged to the average loss values of 1.953×10^{-3} and 3.568×10^{-3}, respectively. Figure 4 shows the loss convergence evolution of the network's 60 training iterations (i.e., epochs) for both the training and validation sets. The maximum and minimum loss value evolutions of the validation datasets are presented in Fig. 5.

Figure 6 depicts example results of the RNN's volumetric flow rate prediction for the training, validation, and test cases. All points fall on or near the true values, indicating a high-fidelity level of model accuracy. By integrating the volumetric flow rate and multiplying it with the density of water, a comparison was made between the predicted and measured total expelled water masses. Table 1 presents the errors between the predicted and measured masses for different common-rail pressure and spray pulse duration cases in the test datasets, with an average error of 7.05%.

This model will be combined with another model describing the relationship between the flow rate and heat flux. With the combined model, correlations between the spray parameters, heat flux, and/or surface temperature can be found, allowing the heat flux to be predicted for a given spray pressure and duration. Furthermore, the relationship

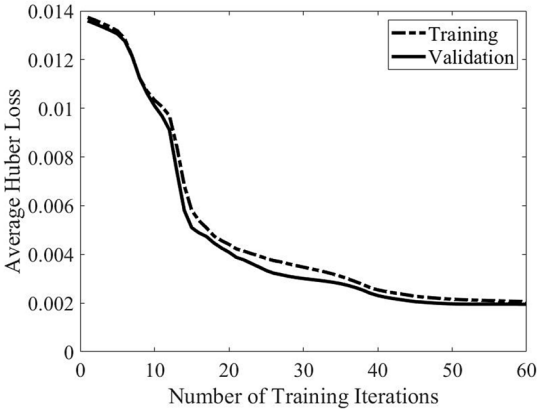

Fig. 4 Average Huber loss vs iterations of the training and the validation datasets.

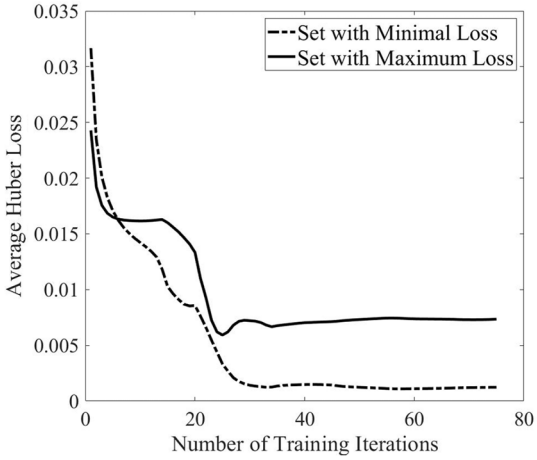

Fig. 5 The maximum and minimum Huber losses vs training iterations in the validation datasets.

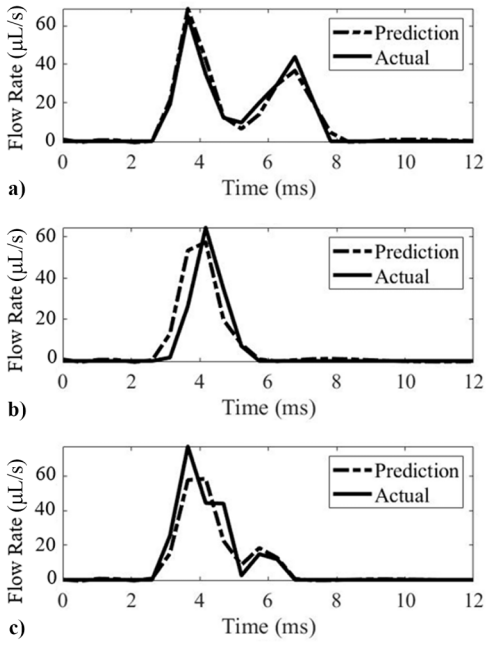

Fig. 6 Volumetric flow rate prediction of a) training, b) validation, and c) test datasets.

Table 1 Errors between predicted and measured total masses for different common-rail pressure and spray pulse duration settings

Pressure, psi	Duration, ms	Calculated mass, μg	Predicted mass, μg	Error of mass, %
1600	4	148.0	140.5	5.4
1400	5	171.5	163.8	4.7
1800	3	115.5	103.7	11.4
1900	3	116.2	107.0	8.6
2100	2	81.5	85.9	5.1

between the PWM signal, the common-rail pressure, and the heat flux/surface temperature can be used to design advanced feedback controls for multinozzle, pulsed, spray cooling systems to achieve uniform mechanical and chemical properties in the cooling process.

The main obstacle of this study is that there are no accurate cost-efficient means of measuring real-time piezoelectric injection volumetric flow rates due to the small magnitude and duration time. Due to the significant delay of the digital scale and its small maximum sampling frequency of 4 Hz, the injected mass could not be measured in real time. Consequently, a linear relationship between the injected mass and the common-rail pressure was assumed based on experiment observation as shown in Eq. (1). However, the total mass or volume per injection event is accurate. Additionally, the NI 9751 driver module limited the maximum injection duration. Therefore, this study was only able to model the injector volumetric flow rate for spray durations of up to 5 ms.

V. Conclusions

This Note develops a data-driven RNN model, mapping PWM control signals and common-rail pressure to the volumetric flow rate of an accumulator-common-rail-injection subsystem in a multinozzle spray cooling testbed. Covering a wide range of experiment scenarios, the predicted flow rate profiles correspond very well to the true values, with an average error of 7.05% in predicting the total volume/mass. The achieved model will be used for advanced spray control methods for the testbed in the future, although it is also anticipated that this work can benefit piezoelectric injection research in engines.

Acknowledgments

This work was supported by the National Science Foundation (grant number 2032764). The authors would like to thank Christopher Souchik for his introduction of the recurrent neural network method.

References

[1] Liang, G., and Mudawar, I., "Review of Spray Cooling—Part 1: Single-Phase and Nucleate Boiling Regimes, and Critical Heat Flux," *International Journal of Heat and Mass Transfer*, Vol. 115, Dec. 2017, pp. 1174–1205. https://doi.org/10.1016/j.ijheatmasstransfer.2017.06.029

[2] Gao, X., and Li, R., "Spray Impingement Cooling: The State of the Art," *Advanced Cooling Technologies and Applications*, edited by S. M. Sohel Murshed, IntechOpen, London, 2019, Chap. 3. https://doi.org/10.5772/intechopen.80256

[3] Liu, P., Kandasamy, R., and Wong, T. N., "Experimental Study and Application of an Artificial Neural Network (ANN) Model on Pulsed Spray Cooling Heat Transfer on a Vertical Surface," *Experimental Thermal and Fluid Science*, Vol. 123, May 2021, Paper 110347. https://doi.org/10.1016/j.expthermflusci.2021.110347

[4] Amon, C. H., "MEMS-Based Thermal Management of High Heat Flux Devices for Integrated Cooling of Electronics," *Ninth Intersociety Conference on Thermal and Thermomechanical Phenomena in Electronic System*, Vol. 2, IEEE, New York, June 2004, Paper 704. https://doi.org/10.1109/ITHERM.2004.1318360

[5] Ravikumar Bandaru, S. V., Villanueva, W., Thakre, S., and Bechta, S., "Multi-Nozzle Spray Cooling of a Reactor Pressure Vessel Steel Plate for the Application of Ex-Vessel Cooling," *Nuclear Engineering and Design*, Vol. 375, April 2021, Paper 111101. https://doi.org/10.1016/j.nucengdes.2021.111101

[6] Zhao, R., Cheng, W. L., Liu, Q. N., and Fan, H. L., "Study on Heat Transfer Performance of Spray Cooling: Model and Analysis," *Heat Mass Transfer*, Vol. 46, Oct. 2010, pp. 821–829. https://doi.org/10.1007/s00231-010-0632-4

[7] Sehmbey, M. S., Chow, L. C., Hahn, O. J., and Pais, M. R., "Effect of Spray Characteristics on Spray Cooling with Liquid Nitrogen," *Journal of Thermophysics and Heat Transfer*, Vol. 9, No. 4, 1995, pp. 757–765. https://doi.org/10.2514/3.735

[8] Pellizzari, N., Touzjian, R., Scouras, A., and Flaherty, W. P., "System-Level Impingement Cooling with Cryogens," *Journal of Thermophysics and Heat Transfer*, Vol. 37, No. 3, July 2023, pp. 579–583. https://doi.org/10.2514/1.T6574

[9] Satkoski, C. A., Shaver, G. M., More, R., Meckl, P., Memering, D., Venkataraman, S., Syed, J., and Carmona-Valdes, J., "Dynamic Modeling of a Piezoelectric Actuated Fuel Injector," *Journal of Dynamic Systems, Measurement, and Control*, Vol. 133, No. 5, Sept. 2011, Paper 051011. https://doi.org/10.1115/1.4003095

[10] Pogulyaev, Y. D., Baitimerov, R. M., and Rozhdestvenskii, Y. V., "Detailed Dynamic Modeling of Common Rail Piezo Injector," *Procedia Engineering*, Vol. 129, Jan. 2015, pp. 93–98. https://doi.org/10.1016/j.proeng.2015.12.014

[11] Abo-Elfadl, S., Ali, A. S., and Siliman, M. H., "Modeling and Simulation of the Common Rail Fuel Injection System of the Diesel Engine," *2017 13th International Computer Engineering Conference (ICENCO)*,

IEEE, New York, 2017, pp. 134–140.
https://doi.org/10.1109/ICENCO.2017.8289777

[12] Haghani, A., Jeinsch, T., Roepke, M., Ding, S. X., and Weinhold, N., "Data-Driven Monitoring and Validation of Experiments on Automotive Engine Testbeds," *Control Engineering Practice*, Vol. 54, Sept. 2016, pp. 27–33.
https://doi.org/10.1016/j.conengprac.2016.05.011

[13] Yu, M., Tang, X., Lin, Y., and Wang, X., "Diesel Engine Modeling based on Recurrent Neural Networks for a Hardware-in-the-Loop Simulation System of Diesel Generator Sets," *Neurocomputing*, Vol. 283, March 2018, pp. 9–19.
https://doi.org/10.1016/j.neucom.2017.12.054

[14] Zuo, Z., Zhang, Y., and Du, M., "Prediction Method of Multi-Injection Pressure Fluctuation of Diesel Engine Based on Recurrent Neural Network Model," *9th International Symposium on Computational Intelligence and Industrial Applications (ISCIIA2020)*, Beijing Inst. of Technology, Beijing, China, 2020.

[15] Yamasaki, Y., Ikemura, R., Takahashi, M., Shimizu, F., and Kaneko, S., "Simple Combustion Model for a Diesel Engine with Multiple Fuel Injections," *International Journal of Engine Research*, Vol. 20, No. 2, 2019, pp. 167–180.
https://doi.org/10.1177/1468087417742

[16] Xu, L., Bai, X. S., Jia, M., Qian, Y., Qiao, X., and Lu, X., "Experimental and Modeling Study of Liquid Fuel Injection and Combustion in Diesel Engines with a Common Rail Injection System," *Applied Energy*, Vol. 230, Nov. 2018, pp. 287–304.
https://doi.org/10.1016/j.apenergy.2018.08.104

[17] Grahn, M., Johansson, K., and McKelvey, T., "Data-Driven Emission Model Structures for Diesel Engine Management System Development," *International Journal of Engine Research*, Vol. 15, No. 8, 2014, pp 906–917.
https://doi.org/10.1177/1468087413512308

[18] Lee, S. Y., Tama, B. A., Choi, C., Hwang, J. Y., Bang, J., and Lee, S., "Spatial and Sequential Deep Learning Approach for Predicting Temperature Distribution in a Steel-Making Continuous Casting Process," *IEEE Access*, Vol. 8, Jan. 2020, pp. 21,953–21,965.
https://doi.org/10.1109/ACCESS.2020.2969498

[19] Awais, M. M., Aamir, M. A., and Aamir, A., "Application of Artificial Neural Networks Modelling to Spray Impingement Heat Transfer," *IEEE International Multi Topic Conference, 2001, Technology for the 21st Century*, IEEE, New York, 2001, pp. 282–291.
https://doi.org/10.1109/INMIC.2001.995352

[20] Nikzadfar, K., and Shamekhi, A. H., "Investigating the Relative Contribution of Operational Parameters on Performance and Emissions of a Common-Rail Diesel Engine Using Neural Networks," *Fuel*, Vol. 125, June 2014, pp. 116–128.
https://doi.org/10.1016/j.fuel.2014.02.021

[21] Wang, J. X., Li, Y. Z., Li, G. C., and Ji, X. Y., "Ground-Based Near-Space-Oriented Spray Cooling: Temperature Uniformity Analysis and Performance Prediction," *Journal of Thermophysics and Heat Transfer*, Vol. 33, No. 3, 2019, pp. 617–626.
https://doi.org/10.2514/1.T5547

[22] Paszke, A., Gross, S., Massa, F., Lerer, A., Bradbury, J., Chanan, G., Killeen, T., Lin, Z., Gimelshein, N., Antiga, L., and Desmaison, A., "PyTorch: An Imperative Style, High-Performance Deep Learning Library," *Advances in Neural Information Processing Systems*, Curran Assoc., Red Hook, NY, Vol. 32, 2019, pp. 8024–8035.

[23] Pincock, C., "The derivation of Poiseuille's Law: Heuristic and Explanatory Considerations," *Synthese*, Vol. 199, Dec. 2021, pp. 11,667–11,687.
https://doi.org/10.1007/s11229-021-03306-1

[24] Laugier, A., and József, G., "Derivation of the Ideal Gas Law," *Journal Chemical Education* Vol. 84, No. 11, Nov. 2007, Paper 1832.
https://doi.org/10.1021/ed084p1832

[25] Hrnjica, B., and Mehr, A. D., "Energy Demand Forecasting Using Deep Learning," *Smart Cities Performability, Cognition, and Security*, edited by F. Al-Turjman, Springer International, New York, 2020, pp. 71–104.

[26] Le, Q. V., Ngiam, J., Coates, A., Lahiri, A., Prochnow, B., and Ng, A. Y., "On Optimization Methods for Deep Learning," *Proceedings of the 28th International Conference on Machine Learning*, Omnipress, Madison, WI, 2011, pp. 265–272.